Invited paper at the
"9th Solid-Vacuum
Interface Conference",
Delft, Holland (1980)

ISTITUTO NAZIONALE DI FISICA NUCLEARE
Laboratori Nazionali di Frascati

LNF-80/67(P)
2 Dicembre 1980

A. Bianconi:

SURFACE X-RAY ABSORPTION SPECTROSCOPY: SURFACE EXAFS AND SURFACE XANES.

Servizio Documentazione
dei Laboratori Nazionali di Frascati
Cas. Postale 13 - Frascati (Roma)

INFN - Laboratori Nazionali di Frascati
Servizio Documentazione

LNF-80/67(P)
2 Dicembre 1980

A. Bianconi(x): SURFACE X-RAY ABSORPTION SPECTROSCOPY: SURFACE EXAFS AND SURFACE XANES (o)

ABSTRACT.

Experimental methods to measure the surface X-ray absorption spectra are described. Physical information that can be extracted from the surface X-ray Absorption Near Edge Structures (XANES) and from the surface Extended X-ray Absorption Fine Structures (EXAFS) is discussed. Applications of this spectroscopy on the local structure determination of surface chemisorption sites and of clean crystal surfaces are reported.

1. - INTRODUCTION.

Diffraction techniques have long been the major means of obtaining structural information. It has been recently found that X-ray absorption spectroscopy is a powerful tool in determining the local structure near a particular atom[1]. This feature makes X-ray absorption spectroscopy a very attractive technique for studing surface structures.

The difficulty of determining surface structure with standard techniques is one of the greatest barriers to development of a better understanding of surface electronic states and surface chemical activity. In fact, the standard structural probes like X-ray and high-energy electron diffraction have no surface sensitivity. Low-energy electron diffraction (LEED)[2] is essentially the only established technique for structure determination, but this technique is limited to surface structures with a long-range order.

Recently the availability of high flux X-ray beams, emitted by high energy electron storage rings have allowed experiments of X-ray absorption spectroscopy of very dilute systems as biological molecules and crystal surfaces. The flux of X-rays from synchrotron radiation can be

---

(x) - Also at Istituto di Fisica dell'Università di Roma, and Istituto di Fisica dell'Università di Camerino.

(o) - Invited paper at the "9th Solid-Vacuum Interface Conference", Delft, Holland, May 7-9, 1980; to be published on Applications of Surface Science.

10^6 times greater than those obtained from bremsstrahlung radiation of X-ray tubes. Several techniques, which have been proposed to measure the surface X-ray absorption spectra of crystals using synchrotron radiation sources, will be described here.

The surface X-ray absorption spectra of a core level of a surface atom can be devided in two parts: the X-ray Absorption Near Edge Structures (XANES) and the Extended X-ray Absorption Fine Structure (EXAFS). From the analysis of the XANES and of the EXAFS structural information like the site symmetry, chemical bonding, interatomic distance and the coordination number can be extracted[1]. This spectroscopy can give information on local structures of systems where LEED has no sensitivity, such as amorphous surfaces and adsorbates without long range order. Moreover interatomic distances in some cases can be determined with an accuracy better than with LEED.

In this paper the experimental techniques for measuring surface EXAFS and surface XANES are reported. The data analysis of surface EXAFS and surface XANES to obtain structural information are described. The limitations and perspectives of these spectroscopies are discussed. Experimental results on surface structure determination of adsorbates on single crystal surface, of amorphous surface oxide layers and of clean single crystal surface are reported.

2. - SURFACE X-RAY ABSORPTION SPECTRA.

The X-ray absorption spectra concern the electronic transitions from atomic core levels to unoccupied final states. The photoabsorption coefficient is given by the product of the density of states D(E) and the matrix element M(E)

$$M(E) = \Sigma \left| \langle f_N \left| \sum_{j=1}^{N} \vec{r}_j \cdot \hat{\varepsilon} \right| i_N \rangle \right|^2 \qquad (1)$$

where $|i_N\rangle$ and $|f_N\rangle$ are the initial and final states of the many N-electrons system with energies E_i and E_f ($h\nu = E_f - E_i$) and the dipole approximation has been employed in treating the radiation field, with the polarization in the direction $\hat{\varepsilon}$. Using the one electron approximation only a primary inner shell photoionization channel is considered and the absorption coefficient given be the golden rule is:

$$\alpha \sim \omega^3 \left| \langle k \left| r \cdot \hat{\varepsilon} \right| K \rangle \right|^2 \qquad (2)$$

where $|K\rangle$ is the core state of the absorbing atom (the central atom) and $|k\rangle$ is the emitted electron state (the internal photoelectron) with wave number k. The local character of this spectroscopy arises from the fact that the matrix element is determined mainly by the radial part of electron wavefunctions. This matrix element is not zero only over the atomic spatial region where the core state radial wavefunction of the central atom is not zero. Therefore only the local character of the final state wavefunction affects the core matrix element.

Generally the binding energy of core levels are one separated from the others by a large energy range, therefore an X-ray absorption spectrum concerns a specific core level on a specific atom. This spectrum is superimposed on an absorption background due to transitions to high energy continuum states from other occupied levels of the same atom and of the other atoms.

Surface X-ray absorption spectra are due to photoionization of core levels of surface atoms. The experimental problem is to distinguish the core transitions in surface atoms from that in the bulk. The problem is simpler when a different atom is adsorbed on the surface, because at the photon energy of its absorption threshold all the absorption structures are due only to surface atoms. However the signal due to surface atoms is a small signal which has to be separated from a large background due to bulk atoms. The experimental methods to measure the surface X-ray absorption spectra enhance the signal from surface atom photoionization processes and should give spectra with a good signal-to-noise ratio. These methods are described in Section 3.

Three parts of a surface X-ray absorption spectrum can be distinguished:

a) The absorption edge is the absorption jump where the first core transitions are energetically allowed. The line shape of the absorption edge and the structures in the photon energy range within a few eV are determined by many body, density of states and/or core excitons effects.

b) XANES extends over an energy range of some tens of eV above the absorption edge where strong peaks with a fine structure appear before the threshold of the EXAFS oscillations[3, 4]. This energy range is defined as that where the excited electron has enough kinetic energy to be in the continuum but its wavelenght is larger than the interatomic distance between the central atom and its first neighbours. At such low kinetic energy the excited electron is strongly scattered by neighbour atoms and its wavefunction is determined by multiple scattering effects inside a cluster formed by the first coordination shell and eventually the second and third shells.

The XANES of simple molecules have been measured[5] and have been interpreted[6, 7] as due to unoccupied valence orbitals and shape resonances. In Fig. 1 the initial core states and the final states relevant in the XANES of a simple molecule like CF_4 or SF_6 are pictorially drawn. The shape resonances arise from the multiple scattering of the excited electron from the central atom in an effective coulomb plus centrifugal potential. In Fig. 2 a pictorial view of the scattering processes of the excited electron in the XANES and EXAFS range is drawn. In the XANES the excited electron is backscattered many times by neighbour atoms at the resonance energies due to the high backscattering probability A(k) at low k values.

Because the XANES spectra are determined by the local site symmetry and are independent on the crystalline order, they can be used to extract information on site symmetry and chemical bonding of unknown compounds[3, 8] and of surface molecular complexes.

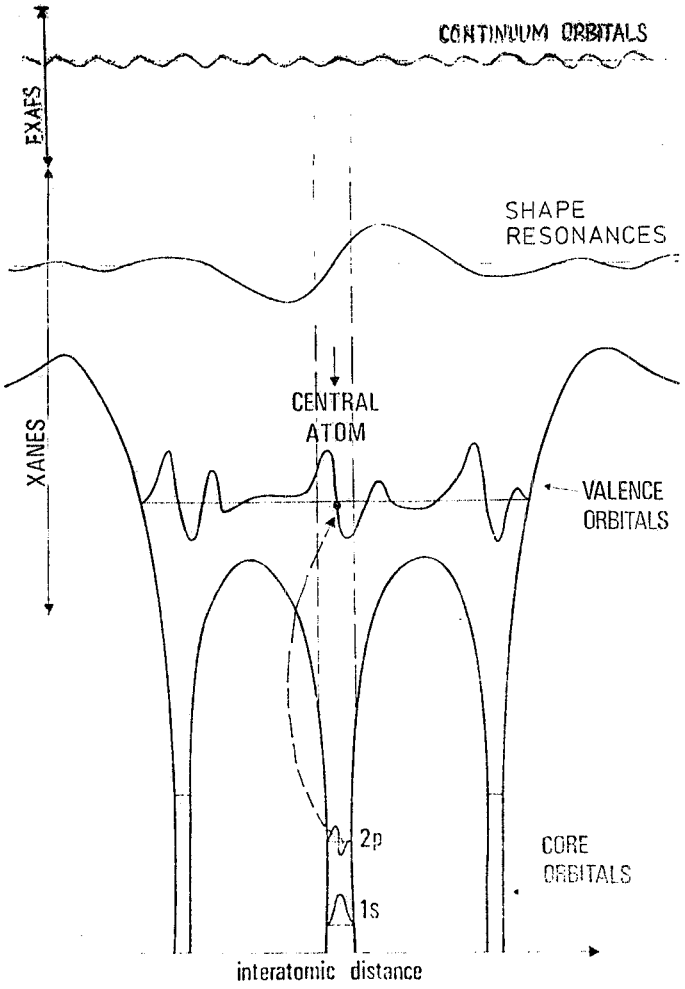

FIG. 1 - Pictorial view of the core initial states and of the final state radial wavefunctions for core transitions. The core excitation takes place in an effective molecular potential seen by the excited electron in the molecular environment. In the case of a molecular cluster like SiO_4 (the microscopic structural unit of SiO_2 oxides) or of simple molecules like CF_4 or SF_6 the XANES spectrum of the absorbing central atom is determined by core transitions to unoccupied valence and to quasi-bound states in the continuum (shape resonances).

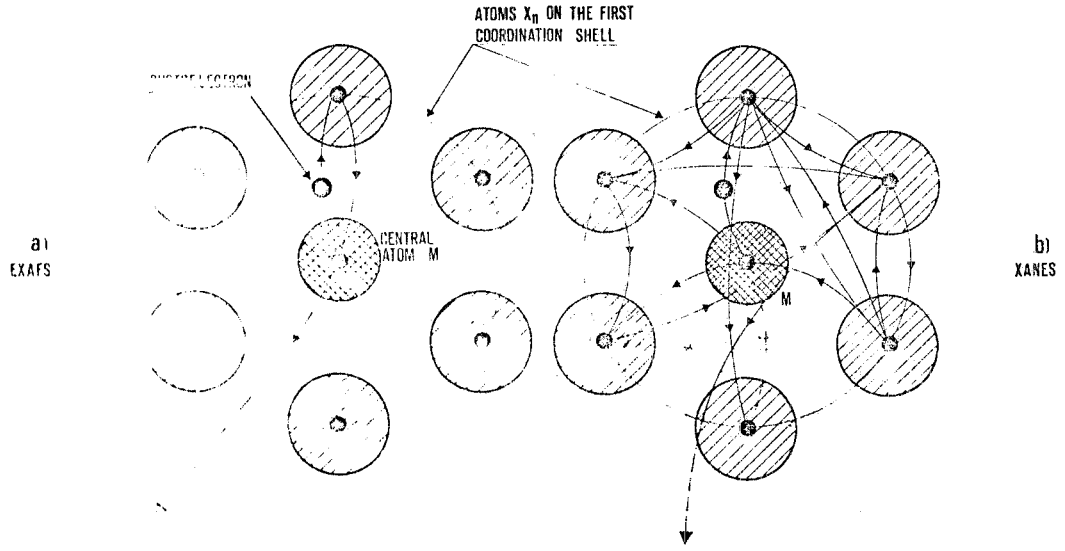

FIG. 2 - Pictorial view of the scattering processes of the internally excited photoelectron determining the EXAFS oscillations and the resonances in the XANES, through matrix element effects.

c) EXAFS spectrum extends from ~40 eV to ~800 eV above the absorption threshold. The study of these weak modulations of the atomic absorption coefficient requires low resolution ($\Delta E \sim$ ~6 eV) and very high signal-to-noise ratio spectra over a large photon-energy-range. The theory of bulk EXAFS[9, 10] is now well established and EXAFS is now used as a standard technique to measure interatomic distances and coordination numbers.

In the EXAFS range the kinetic energy of the excited internal photoelectron from the central atom M is high enough that the plane wave approximation is good and it is weakly scattered, with the backscattering probability A(K), by a single neighbour atom (see Fig. 2). Interference effects between the outgoing and backscattered wavefunction of the excited photoelectron through matrix element effects induce a modulation of the absorption coefficient.

Many body effects[11] and the introduction of spherical waves in the place of plane waves[12] have to be considered to explain fine details in the analysis of the amplitude of EXAFS oscillations, as has been pointed out recently.

For the applications of EXAFS to structural analysis, the important point is that, following a standard procedure of data analysis, reliable interatomic distances and coordination numbers can be obtained with high accuracy.

EXAFS spectroscopy gives information only on the local structure around the absorbing atom within a distance of about 5 Å from it. Such a local sensitivity is determined by the inelastic electron scattering mean free path and by the Debey-Waller factor.

3. - EXPERIMENTAL METHODS.

3.1. - X-ray transmission.

Bulk X-ray absorption spectra are usually measured by the standard X-ray transmission measurements through thin 0.1 - 1 μm films. Because $\varepsilon_1 \approx 1$, the absorption coefficient is $\alpha(h\nu) = 1/d \ln I_0/I$ where d is the sample thickness and I_0 and I are respectively the incident and trasmitted flux. The number of atoms of a surface monolayer on a crystal surface are only about 10^{13} in the X-ray beam, surface effects are therefore generally negligible in bulk transmission measurements.

There is a special system where X-ray transmission can be used to record surface EXAFS and surface XANES. The system where the substrate is nearly completly transparent at the photon energy of the absorption edge of chemisorbed atoms and the effective surface area of the substrate is very large. This special substrate is "grafoil". The surface spectra of heavy atoms like Br_2 and Kr on graphite have been measured using this technique and good signal-to-noise data have been obtained[13].

3.2. - X-ray reflection.

Below the critical angle for total reflection, the reflectivity is high (> 50 %) and the penetration depth for X-rays is low (20-100 Å), therefore this technique is surface sensitive. The

critical angle is about 0.5° at 10 keV rising to 5° at 200 eV.

First experimental evidence of EXAFS oscillation on X-ray reflection spectra has been given by Barchewitz et al.[14]. The EXAFS of the graphite surface layer on the grating of a soft X-ray monochromator due to carbon contamination has been extracted by the output spectrum of the monochromator[15]. Good signal-to-noise spectra of very good optically polished crystal surfaces have been recently measured[16] and a theoretical calculation of the X-ray reflection spectra has been done[17]. This promising technique has not jet been applied to interesting problems.

3.3. - Techniques recording core hole decay products.

The inner shell photoionization process can be described as a two steps process. In the first step the photon excites a core hole-excited electron pair, and in the second step the recombination process of the core hole takes place. There are many channels for the core hole recombination, each one with a probability p_i, and each channel produce the emission of photons or electrons and ions which can be collected with a special experimental apparatus. Assuming that the two steps are independent on photon energy the recorded number of the decay products of a special decay channel will be proportional to the number of core hole produced in the sample by the X-rays which is proportional to the absorption coefficient.

The recombination channel which has been used to record bulk X-ray absorption spectra of dilute systems is the direct radiative core hole decay producing X-ray fluorescence lines[18]. The X-ray fluorescence lines have high photon energies and therefore this technique probes the bulk.

The main recombination channel selected for surface X-ray absorption is the non-radiative decay channel of the core hole followed by electron emission from the sample surface in the vacuum (Auger process). A typical experimental set up is shown in Fig. 3 and in Fig. 4. The electrons emitted into the vacuum originate from a surface layer of thickness Λ which is determined by the electron kinetic energy through the effective escape depth l(E). The electron escape depth is a strong function of the electron energy and is also dependent on the material. The effective escape depth for low kinetic energy electrons in a metal (Al) and in a semiconductor (GaAs) is

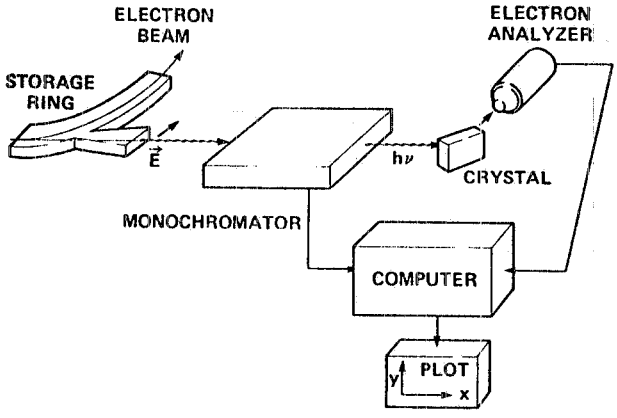

FIG. 3 - Experimental set up for surface X-ray absorption measurements using synchrotron radiation and electron yield or angular integrated constant initial state CIS detection modes. For the "total yield" method the electron energy analyser is substituted by a simple channeltron electron multiplier.

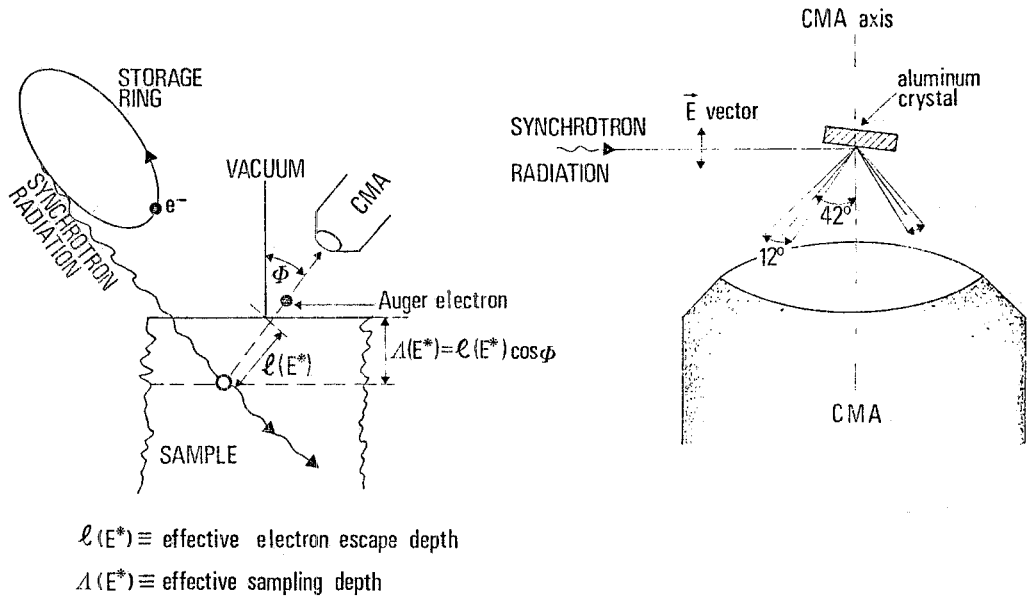

$\ell(E^*) \equiv$ effective electron escape depth

$\Lambda(E^*) \equiv$ effective sampling depth

FIG. 4 - Experimental set up for surface EXAFS measurements using electron yield techniques with polarized synchrotron radiation. This geometry has been used for Auger yield and secondary partial yield. The EXAFS of clean Al surface, using the intermediate partial yield method, and of graphite surface, using the CIS detection mode, have been studied with this geometry.

plotted in Fig. 5. The number of emitted electrons is proportional to the number of core hole N_h created by the X-ray beam in a surface layer

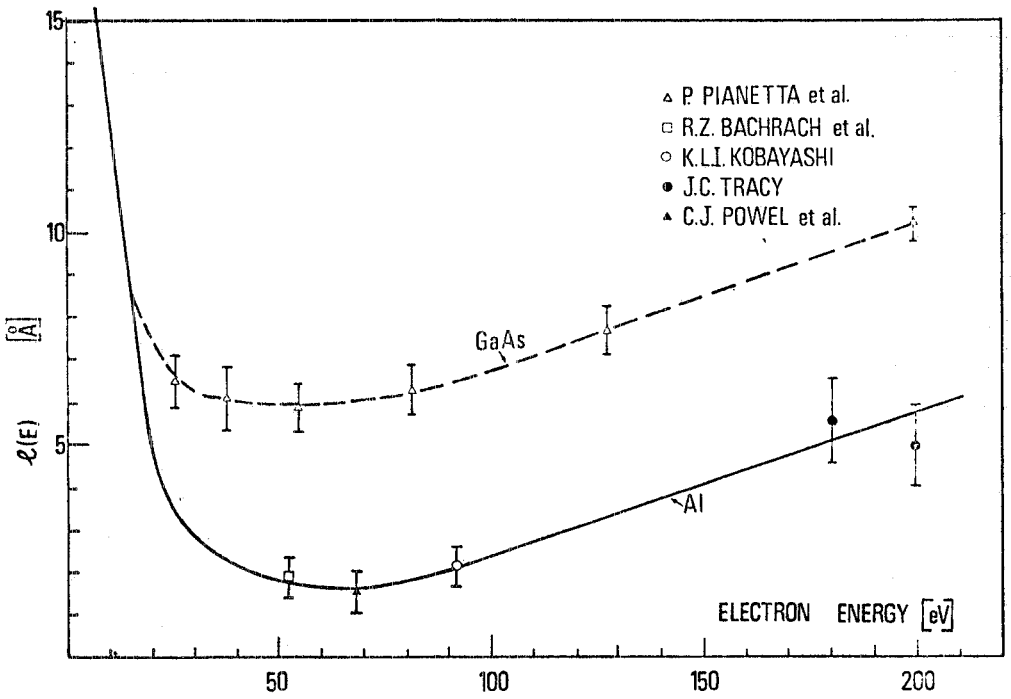

FIG. 5 - Measured effective electron escape depth in Al and GaAs. The data have been taken from refs. (19-22). See ref. (23) for silicon.

$$N_h = N_o \alpha_c \Lambda \qquad \text{where} \quad \alpha_c \approx N_s \sigma_c \qquad \text{if} \quad \alpha_c \Lambda \ll 1$$

N_o is the number of incident photons, α_c the absorption coefficient, N_s is the surface density of atoms and σ_c the core photoionization cross section.

The surface sensitivity can be defined as the ratio between the parts of the signal due to the surface layer and that due to the substrate. This quantity is depending on the selected decay channel and in the case of electrons on the effective escape depth plotted in Fig. 5.

The signal-to-noise ratio is depending on the number of events which can be detected. The number of counts due to a monolayer of thickness d is $N_o \alpha_c d p \Omega$, where p is the probability of the selected channel of the core hole recombination and Ω is the solid angle collected by the detector. An important part of the apparatus determining the signal-to-noise ratio, through N_o, is the optical set up including X-ray mirrors, X-ray monochromators and high current storage rings[24]. Other important parameters are the detection solid angle, the efficiency of detectors and the selected core hole decay channel.

It is important to remark that the requirements for good surface XANES and surface EXAFS spectra are different. The resolution of the X-ray spectra, determined by the optical set up (monochromators and mirrors) should be high ($\Delta E \lesssim 1$ eV) for the XANES and can be low for EXAFS ($\Delta E \sim 6$ eV). The signal-to-noise ratio should be very high for the weak EXAFS modulations to obtain interatomic distances with good accuracy, while it is a less severe requirement for the strong XANES resonances.

3.3.1. - Auger electron yield.

In the soft X-ray range, $h\nu < 4000$ eV, the Auger recombination has higher probability than the radiative recombination. As the energy of Auger electrons is characteristic of a particular atom, it was suggested[25,26] that the selective photoabsorption cross section of atomic species chemisorbed on a surface could be measured by monitoring the intensity of its Auger electrons as a function of photon energy. The basic phenomena which justify this detection technique are that the Auger emission is nearly isotropic and the energy of Auger electrons does not change as a function of photon energy. An intense Auger line is selected by an electron analyser, operated in the constant final state mode (CFS) with an energy window of a few eV.

A standard experimental set up for this type of surface X-ray absorption measurements is shown in Fig. 3. The surface contrast of this technique is determined by the ratio between the intensity of the Auger line and the secondary electron background at the same energy coming from the substrate. In Fig. 6 is given a pictorial view of the evolution of the energy spectrum of emitted photoelectrons (EDC's curves) as a function of the energy of exciting photons. The measured variation of the EDC curve of aluminum with the appearence of the Auger band for photon energy above the $L_{2,3}$ threshold is shown in Fig. 7.

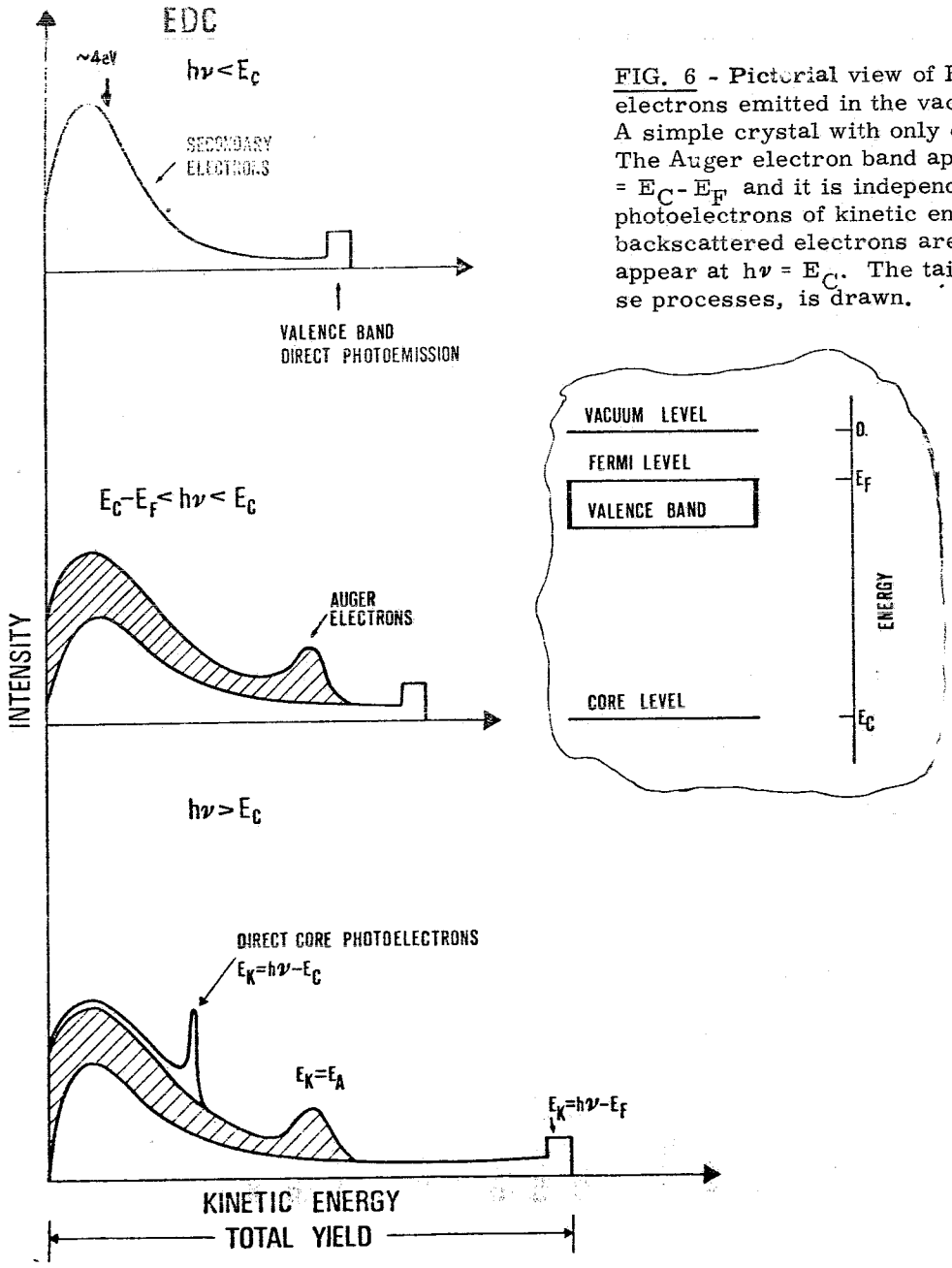

FIG. 6 - Pictorial view of Electron energy Distribution Curves (EDC) of photoelectrons emitted in the vacuum at three different photon excitation energies $h\nu$. A simple crystal with only one valence band and one core level is considered. The Auger electron band appear at the core photoabsorption threshold $h\nu = E_C - E_F$ and it is independent on the photon energy. The direct valence band photoelectrons of kinetic energy $E_K \sim h\nu - E_F$ with their tail of secondary backscattered electrons are always present. The direct core photoelectrons appear at $h\nu = E_C$. The tail of secondary electrons, originated by each of these processes, is drawn.

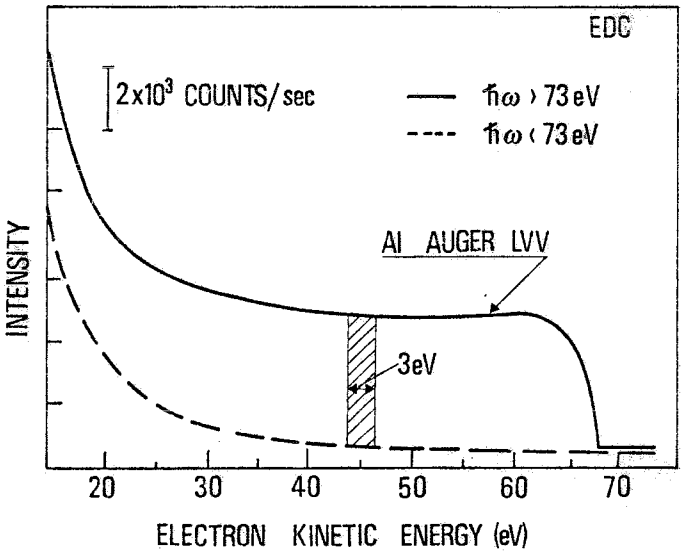

FIG. 7 - EDC of $L_{2,3}$ Auger electrons in Al excited by photon energies above and below the absorption edge at 73 eV.

3. 3. 2. - Total electron yield.

The measurement of the total electron yield has been found to be proportional to the bulk absorption coefficient in the soft X-ray range using standard sources[27, 28] and synchrotron radiation[29]. This technique has recently been applied in the hard X-ray range 8-10 keV using a crystal monochromator[30]. This technique measures the integral over the entire energy range of the electron energy distribution curves (EDC), see Fig. 6.

The surface contrast of this technique is poor because both low energy secondary electrons and high energy photoelectrons are collected. In the hard X-ray range[30] it was estimated that about 100 Å contribute to the recorded signal. The advantage of this method is that the maximum counting rate is obtained since all emitted electrons over 2π sterad can be collected by giving a positive voltage on the detector, which in this case is only a high current channeltron electron multiplier.

This detection technique has been found to be the one giving the best signal-to-noise ratio between the electron yield techniques for surface EXAFS of Oxygen on Al[31, 32].

3. 3. 3. - Low-energy-electron partial yield.

It was proposed to improve the surface contrast of the total yield method by measuring only the secondary electrons within a kinetic energy window around 4 eV (see Fig. 6)[33]. Selecting only secondary electrons of this kinetic energy the surface sensitivity is higher than that of the total yield. About 20 Å of the sample contribute to the spectrum. The counting rate is high because the kinetic energy is close to the maximum of the secondary EDC[34]. Fig. 6 shows that the increase of the signal in the secondary yield at the core threshold $h\nu_0 = E_F - E_C$ is due to inelastically scattered Auger electrons. The basic experimental set up is shown in Fig. 4. The cylindrical mirror analyser (CMA) is operated in the CFS mode.

This technique has been applied to study surface core excitons on clean crystal surfaces of semiconductors[33]. These surface excitons appear as new peaks at lower energy than the bulk absorption threshold. To study surface effects above the absorption edge a more surface sensitive technique is required.

This technique has also been applied to study the thick surface oxide layers, about 20 Å[34] on aluminum and the surface EXAFS of chemisorbed oxygen on metal and semiconductors[35-38]. The K edge of oxygen is in a photon energy range $h\omega \sim 530$ eV, which is difficult to reach experimentally. The spectra quoted above were measured using the "grasshopper" monochromator at SSRL[39] with a fairly low resolution, about 4-10 eV. Therefore it was impossible to measure high resolution XANES but it was ideal for EXAFS which requires only about 6 eV resolution. The counting rate was limited by the channeltron electron multiplier which is easily saturated by the strong background of secondary electrons coming from the substrate. This problem has been partially solved using high current channeltrons[31, 32].

3. 3. 4. - Intermediate-energy electron yield.

The surface contrast can be enhanced by selecting only emitted electrons, with an inter-

mediate kinetic energy between 20 and 100 eV[40]. Fig. 8 shows the surface $L_{2,3}$ spectra of aluminum exposed to 200 Langmuir of oxygen using a CMA and the experimental set up in Fig. 3.

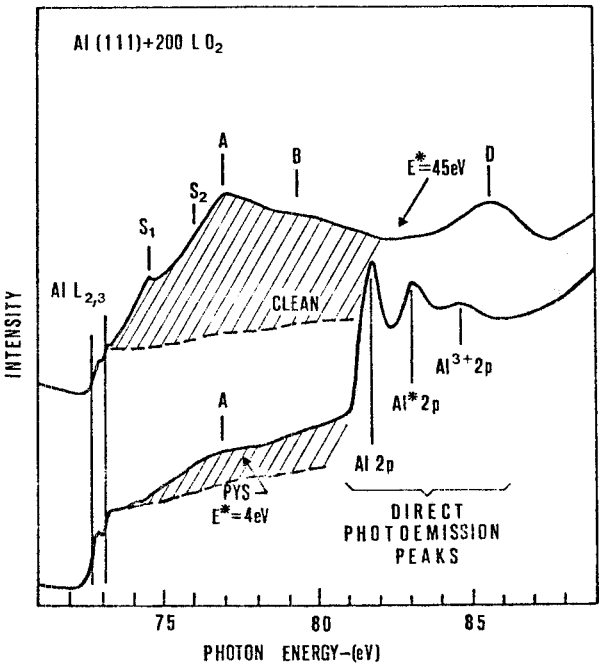

FIG. 8 - Secondary partial yield (E^* = 4 eV) and intermediate energy yield (E^* = 45 eV) giving the surface $L_{2,3}$ soft X-ray absorption spectra of clean Al(111) surface (dashed curve) and of Al(111)+200 Langmuir of chemisorbed O_2 (solid curve). The dashed and solid curves have been normalized at the same intensity at the clean Al threshold (73-74 eV) where the transitions from core levels of Al-O complex are not yet energetically possible. The absorption spectrum due to Al 2p core level of the Al-O complex can be obtained by the difference between solid and dashed curves. Direct core photoemission peaks appear at $h\nu = E^* + E_c$.

The spectra have been taken in the CFS mode E^* = 4 eV and E^* = 45 eV. Clearly the surface contrast, i. e. the ratio between the signal due to chemisorbed oxygen (dashed area) and the signal due to the substrate (dashed curve of clean Al) is strongly increased, in the intermediate energy yield spectrum. This technique gives a spectrum free of interference with core direct photoemission peaks in the range $E_c < h\nu < E_c + E^*$ using the notations of Fig. 6. This will not be the case if there are other atomic species having core levels in this energy range. This technique has been used to measure high resolution XANES[41-45] of chemisorbed atoms or of the first surface oxide monolayer on metals and semiconductors.

A different experimental set up[46] was used to measure the surface EXAFS of oxygen collecting about all electrons ejected in 2π sterad and rejecting all the low energy secondary electrons. Fig. 9 shows a comparison between the spectra taken with this method and with the secondary yield method. The surface contrast is clearly increased and the counting rate decreases by only an order of magnitude. The spectrum was recorded over a 10 hours collection time on the grasshopper beam line of SSRL[39] and the storage ring SPEAR operated at 1.8 GeV and 7 mA giving a photon flux of 10^9 photons/sec within the band-pass of the monochromator. The detector consisted of two hemispherical grids abd a channeltron electron multiplier. The sample and the first internal grid are kept at ground potential and the electrons are retarded by the negative potential on the second grid. Since all electrons below the energy cut off are rejected the low energy secondary electrons coming from the bulk are not collected. The measure of the surface absorption spectra of a clean surface has been obtained

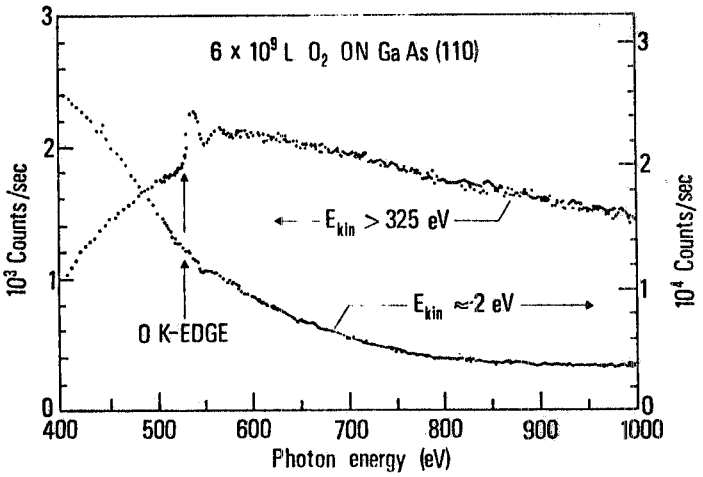

FIG. 9 - Electron yield spectra of the K edge of oxygen on GaAs using retarding field grids. The spectrum taken with a 325 eV low energy low off is compared with the secondary partial yield spectrum. Figure taken from ref. (46).

by the method which gives the highest surface contrast[47]. The technique should detect the Auger electrons of kinetic energy such that the effective escape depth 1(E) is minimum. The measured effective escape depth in aluminum, plotted in Fig. 5, has a minimum of only 2 Å at ~40 eV. Therefore it is possible to measure the surface absorption spectra of the clean surface of aluminum by the CFS mode with the fixed energy window at 45 eV. Fig. 7 shows the EDC of Al excited by photons with energy lower (dashed line) and higher (solid line) than the photoabsorption threshold of the 2p core level $h\nu_0 = E_0 = 73$ eV. A broad band of Auger electrons appears when photons have enough energy to create the 2p hole. The number of direct valence band photoelectrons is much smaller than the number of Auger electrons. Therefore the valence band is hardly observed using the same intensity scale. The experiment was performed at SSRL on the grasshopper line and the storage ring was operated at 2 GeV and 14 mA.

It is possible to increase further the surface contrast by selecting the Auger emission angle and the incidence angle of incoming photon flux. Selecting the emission angle as is shown in Fig. 4 the effective sampling depth is $\Lambda(E^*) = 1(E^*)\cos\phi$. By collecting Auger electrons at the largest possible emission angle $\phi \sim 80^\circ$, $\Lambda(E)$ can be reduced by a factor of 10. The surface contrast can be estimated by the ratio of the total emission of Auger electrons from the first surface layer and that due to all the layers below

$$R = \frac{I_S}{I_{bulk}} = \left\{ \sum_{i=1}^{\infty} \exp - \left[\frac{(i + 0.5)\, a}{\Lambda} \right] \right\}^{-1}$$

assuming a discrete distribution of atomic layers with a spacing a. We have measured the $L_{2,3}$ absorption spectrum of the clean Al(111) surface using $\phi = 42^\circ$, 1(45 eV) = 1.45 Å and a = 2.33 Å the estimated surface contrast R is about 8 i.e. only about 11% of the signal is due to the underlying layers. A different method to define the surface sensitivity is to use a continuum model. It is possible to define the thickness of the surface layer which contribute about 86% of the signal $h = 2\Lambda$.

3. 3. 5. - Photon-stimulated-desorption (PSD).

It has been demonstrated that the photoionization of a core level of an adsorbate induces ion desorption through the interatomic Auger recombination[48, 49]. Because the ion current due to the PSD is proportional to the number of created core holes, i. e. to the photoabsorption cross section of the adsorbate, it is a measure of the surface absorption with a very high surface contrast in comparison with the already discussed detection methods. The experimental set up will be formed by a mass spectrometer selecting the ions produced by PSD of the corresponding adsorbed species.

Recently a good signal-to-noise ratio spectrum of surface EXAFS of O_2 on Mo(100) using a simple time-of-flight spectrometer to select the O^+ ions has been reported[50]. The surface XANES of SiO_2 has also been measured recording the H^+ ions emitted from the surface of fused SiO_2[51].

3. 3. 6. - Luminescence yield (surface optical EXAFS).

An alternative approach to measure the surface absorption of a thin oxide layer or of a chemisorbed molecule in the X-ray range is to record the intensity of optical or near UV luminescence emitted by the active surface molecule under the X-ray flux. This method has been used for measuring the bulk X-ray absorption[52] and can be easily applied to study surfaces with the advantage, in comparison with other techniques, that all the emitted optical luminescence can be focused on the photomultiplier using optical mirrors.

3. 4. - Angular integrated constant initial state spectra (CIS).

In constant initial state spectra the intensity of a direct photoelectron peak excited from a core level or the valence band of binding energy E_c (see Fig. 6) is followed by varying the kinetic energy at which photoelectrons are collected $E_{kin} = h\nu - E_c$. The measure of the number of photoelectrons $N(h\nu, E_{kin})$ is proportional to the partial photoionization cross section of selected initial and final states. This photoelectron mode was first proposed by Lapeyre et al.[53] and can be used to obtain various information. Angular resolved CIS can give the dispersion of the valence and conduction bands[54] and structural information through the photoelectron diffraction effects[55, 56].

Angular integrated CIS can give the partial photoionization cross section of the initial state[57-60]. Near the threshold the direct photoemission peak is superimposed on top of the secondary peak (see Fig. 6). In the first 50 eV above the threshold CIS cannot therefore be applied[58, 59] but is possible to use at higher energies[59, 60]. Moreover CIS have to be corrected for the energy dependent transmission of the electron energy analyser. The surface sensitivity of CIS spectra is determined again by the effective escape depth of collected photoelectrons in the kinetic energy range 50-300 eV necessary for a surface EXAFS spectrum and by the fact that only unscattered photoelectrons ejected in the vacuum are collected.

, CIS spectra are proportional to the total photoionization cross section only if all electrons emitted over 4π sterad are collected[26]. Therefore only in this case the standard formula for EXAFS oscillations could be strictly applied. In fact selecting only electrons in one direction photoelectron diffraction effects[55,56] and atomic effects through the asymmetry parameter $\beta(h\nu)$ can induce large deviations from the true total photoabsorption. The number of photoelectrons ejected in a specific direction from an atom by polarized monochromatic radiation has the form

$$N \approx \frac{\sigma}{4\pi}\left(1 + \frac{\beta}{2}(3\cos^2\theta - 1)\right)$$

where σ is the total dipole cross section and θ is the angle between the electric vector of the radiation and the direction of emitted electrons, β is the asymmetry parameter and can exibit large energy dependent variations from the expected value 2[61]. For each type of electron analyser and experimental set up it is important to define the collected solid angle. Using a CMA and experimental set up of Fig. 4 one integrates the emission over all the azimuthal angles and over polar angles between 36^o and 48^o (resulting solid angle 0.88 sterad). Also if this angle is much smaller than 4π we have found that the CIS of the 2s level of graphite shows EXAFS oscillations in agreement with results in other layer compounds[60]. The results will be discussed in the last Section of this article.

3.5. - Extended Appearance Potential Fine Structure Spectra (EAPFS).

Surface EXAFS oscillations have been recently detected in electron excited APS spectra[63,64]. This technique is different from the others since it does not require synchrotron radiation and the core hole is created by incident electrons. The final state energy is divided between two electrons. "Differentiation of the yield with respect to incident energy E_o produces a signal which strongly emphasizes the situation in which one electron is close to the Fermi level. Thus it is the first derivative of the yield which is analogous to undifferentiated absorption spectrum of EXAFS" (from ref. (62)). The measure of EAPFS was obtained with a conventional hemispherical-grid LEED optics by recording the second derivative of the elastic yield as a function of E_o. The retarding grids are biased a few volts positive with respect to the emitter of the electron gun and the second derivative was obtained by superimposing a small sinusoidal oscillation on the sample potential and detecting the second harmonic. In order to analyse the data with the usual EXAFS formula for dipole transitions it is necessary to establish theoretically the connections between the electron and photon cross sections. Fortunately the usual theoretical EXAFS formula can be applied but the final state phase shift in the oxygen K shell excitation is that of the $l = 0$ wave instead of $l = 1$[64]. This method is limited to amorphous surface due to the presence of structures associated with the diffraction effects of the incident beam. Recently[65] this limitation has been overcome by using a solid state soft X-ray detector, recording the soft X-ray yield as the core level de-excites (SXAPS).

4. - SURFACE XANES: DATA ANALYSIS AND EXPERIMENTAL RESULTS.

X-ray Absorption Near Edge Structures XANES extend over an energy range above the absorption threshold E_o where the wave number of the final state electron (the internal photoelectron) is

$$K < 2\pi/R$$

where R is the interatomic distance between the absorbing atom (the central atom) and the first coordination shell, XANES can be determined by atomic or molecular effects if the local character of the final state wavefunction is mainly determined by the atomic potential, or by the molecular potential due to the central atom and its neighbours. Generally atomic effects are large for transitions from core radial wavefunction with nodes. In this case the spectra are dominated by Fano-Cooper minima and delayed transitions[66]. Strong "white lines" of mostly atomic character also appear in the $L_{2,3}$ spectra of transitions metals and rare earths compounds[67]. In these spectra the atomic resonances near the edge are so strong that they obscure molecular effects.

When atomic effects are negligible the XANES is dominated by molecular effects. The final state wavefunctions, as discussed in Section 2 of this paper, are determined by the local structure around the absorbing atom. The XANES, where the excited electrons strongly interact with many atoms (see Fig. 2), contain information on relative orientations and bond angles of atoms surrounding the absorbing atom[4]. For example EXAFS, where single atomic scattering events dominate, only the pairwise atomic correlations are relevant. The molecular complexes formed by chemisorbed atoms on crystal surfaces can have a complex symmetry, therefore the average interatomic distance determined by EXAFS can not be sufficient to determine its structure. Complementary information on banding angles and higher order atomic correlation effects can be obtained from XANES. Second shell effects are also expected to be important in XANES where the final state is in a fully multiple scattering regime.

The important role of the molecular symmetry of the cluster around the central atom is experimentally well established. The XANES of molecules like CF_4, SO_4, $GeCl_4$ are all similar concerning the shape and intensity ratios of the peaks despite the fact that the central and neighbour atoms are different. The symmetry of a molecular cluster can be easily determined by comparing the XANES of an unknown system with that of known systems[3, 8].

The important point for using the XANES as a "fingerprint" of the local structure around the central atom is to determine the role of the long range order. There are several experiments giving evidence for the insensitivity of the XANES spectra to long range order when they are determined mainly by the first coordination shell[3]. A typical example is the $L_{2,3}$ spectrum of SiO_2, characteristic of the SiO_4 tetrahedral microscopic cluster. This spectrum is the same in α-quartz and amorphous silica[43]. The surface XANES of fused SiO_2 also show a symilar spectrum[51] showing that long range order can be disregarded in this case. This experimental evidence has suggested an empirical approach for determining surface local structures by com

paring surface XANES with bulk XANES of known compounds.

Using this approach the structure of the first surface oxide on Si(111) crystal surface has been determined[43]. This oxide is formed by SiO_4 units typical of SiO_2. In fact, as is shown in Fig. 10, the surface XANES of the first oxide on the Si(111) formed at room temperature is similar to bulk SiO_2. Evidence of SiO formation on the Si surface at high temperature has been clearly found. In fact in Fig. 10 the XANES of the surface oxide monolayer grown at high temperature is completely different and is the same as the bulk XANES of SiO[44].

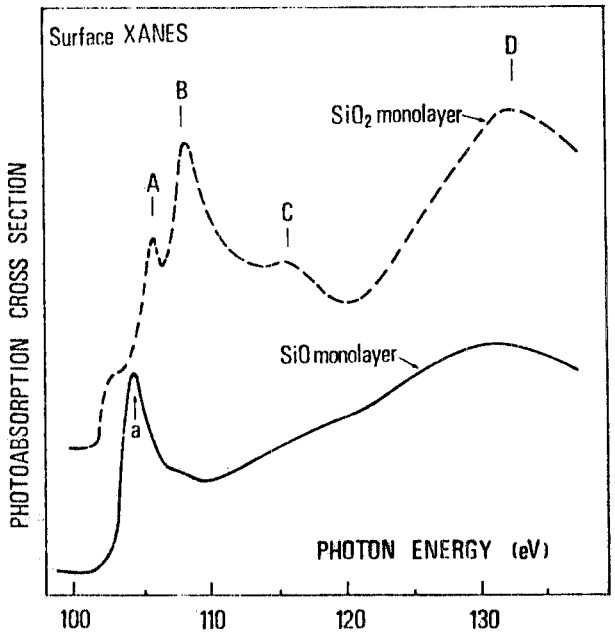

FIG. 10 - Surface XANES of the first oxide layer formed on Si(111) at room temperature ("SiO_2 monolayer") and at high temperature ("SiO monolayer").

The effects of second coordination shell can be important[3, 4]. In the case of SiO_2 second shell effects appear through a variation of the Si-O-Si bridging bond angle. The variation of this angle induces a change on the Si-O effective charge transfer inducing a shift of the initial core state[68]. This effect appears in the surface XANES spectrum of SiO_2 on Si(111) through the energy shift of the peak A, a discrete (excitonic) excited state, of about 1 eV in comparison with bulk XANES of SiO_2. This result indicates a decrease of the average bridging bond angle from the α-quartz value of 144°.

The surface XANES of oxygen chemisorption on the principal crystal faces of Al have been studied[41]. Evidence for the transition from the chemisorbed phase to the oxidation phase has been found. This experiment demonstrates also the local character of XANES spectra because they appear to be determined mainly only by the microscopic $Al\text{-}O_x$ molecular cluster, which changes going from the chemisorption to the oxidation phase.

In order to determine the structure of the first oxide molecular monolayer on Al its XANES spectrum has been compared with bulk $\alpha\text{-}Al_2O_3$ and amorphous alumina, which have tetrahedral and octahedral local symmetry around the Al ion respectively.

The spectra are plotted in Fig. 11[43]. The data show that the local structure of the surface oxide is different from both model compounds but it is close to the spectrum typical of octahedral symmetry. This result is in agreement with surface EXAFS results[31, 32, 74] which gives a longer Al-O distance ($R = 1.88$ Å) in the first Al_2O_3 oxide layer than in the bulk alumina ($R = 1.85$ Å), where the Al ions have mostly a tetrahedral coordination. A longer Al-O interatomic distance is expected for Al coordinated by 6 oxygen atoms than for Al

coordinated by 4 oxygen atoms[74].

This is a typical example to show the different kind of information that can be extracted from the surface XANES and surface EXAFS. XANES is more sensitive to the symmetry and is a useful fingerprint of the local structure, EXAFS gives mainly the value of the interatomic distance which is a fundamental quantity to determine the local structure but it is not enough to determine completely an unknown surface local structure.

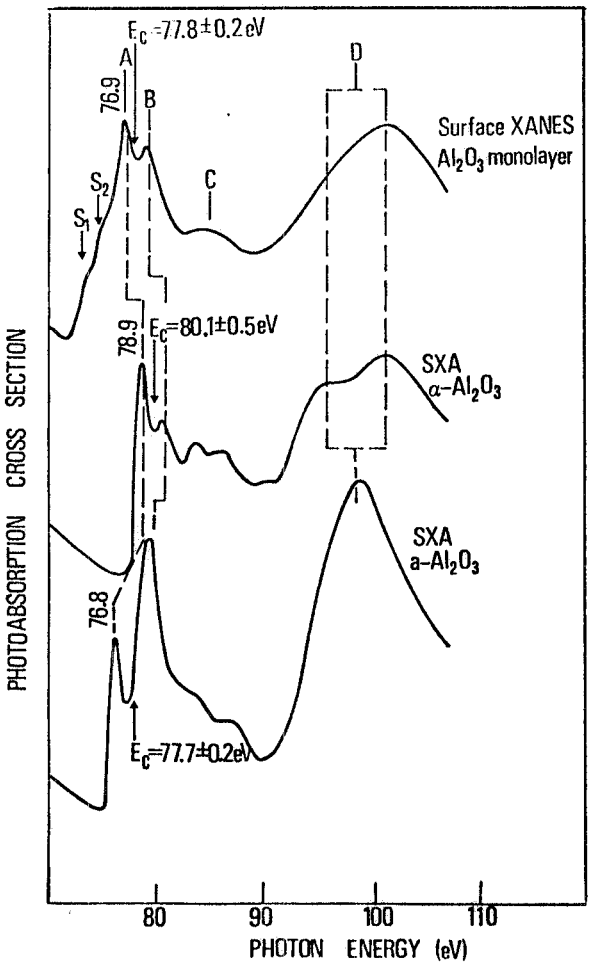

FIG. 11 - Surface XANES of the first oxide monolayer on Al(111), Al(100) and Al(110) surfaces compared with the bulk soft X-ray Absorption (SXA) spectra of model compounds where the Al atom has octahedral (α - Al_2O_3) and tetrahedral (a - Al_2O_3) coordination.

5. - SURFACE EXAFS: DATA ANALYSIS AND RESULTS.

EXAFS is actually a standard technique to measure interatomic distances and coordination numbers[9,10]. The final state interference effects modulate the atomic absorption coefficient α_{ca}. The measured absorption coefficient α is given by the sum of the background absorption α_b and the absorption coefficient due only to the core level α_c

$$\alpha_c = \alpha - \alpha_b$$

The EXAFS modulations are given by

$$k \cdot \chi(k) = \frac{\alpha_c - \alpha_{ca}}{\alpha_{ca}} k$$

where k is the wavevector of the excited electron $k = 0.5123 (\hbar\omega - E_o + V_o)^{1/2}$ Å^{-1} and E_o is the absorption threshold, V_o is the inner potential.

The first step in data analysis is to remove the background α_b, α_b generally is removed by preedge fitting but in surface EXAFS of a chemisorbed atom it can be removed by subtract

ing the surface absorption spectrum of the clean surface. This first step in data analysis is very important because a wrong background subtraction affects the measured coordination number, but fortunately it has a negligible effect on the measured interatomic distance.

In the second step $\chi(k)$ is obtained by removing the smooth atomic background α_{ca}.

The third step in data analysis is to calculate the Fourier transform of the spectrum. Distinct peaks for each coordination shell are obtained.

The fourth step is to isolate the contribution from the individual shells, in order to simplify the analysis of EXAFS. The peak corresponding to the shell of interest is back transformed into k space, where its amplitude A(k) and phase $\phi(k)$ can be determined as a function of k. This experimentally determined EXAFS oscillation due to only one coordination shell should be compared to the theoretical formula[9] of the EXAFS oscillation:

$$k \cdot \chi(k) = (-1)^l A(k) \sin \phi(k)$$

where $\phi(k) = 2kR + \varphi(k)$,

$$A(k) = \left(\frac{N^*}{R^2}\right) F(k) \exp(-2\sigma^2 k^2 + 2R/\lambda(k)) ,$$

in L spectra $l = 2$ and $N^* = 3 \sum_{i=1}^{N} (1/3 + \cos^2 \theta_i)$,

in k spectra $l = 1$ and $N^* = 3 \sum_{i=1}^{N} \cos^2 \theta_i$.

N^* is the effective coordination number and N is the real coordination number; λ is the mean free path for inelastic scattering of the internal photoelectron; A(k) is the backscattering amplitude which is characteristic of each atom and allows the determination of the type of backscattering atoms; σ is the Debey Waller like factor:

$$\varphi(k) = \phi_a(k) + \phi_b(k) = 2\delta^1(k) + \phi_b(k)$$

where δ^1 is the phase shift due to the central atom and ϕ_b the phase of the backscattering amplitude.

The value of the wave number k of the excited photoelectron is depending on the choice of the inner potential V_o. V_o is determined by setting V_o such that the experimental phase at $k = 0$ is the same as the theoretical phase[9].

The more reliable way to determine interatomic distances and to avoid using theoretical phase shift is to measure the bulk EXAFS of a model compound with the same central atom, the same number of near neighbours at about the same distance. The difference between the phase of the model ϕ_m and the experimental $\phi(k)$ is

$$\phi(k) - \phi_m(k) = 2k(R - R_m) .$$

In this way by knowing the distance of the model R_m the unknown distance R can be found.

In surface EXAFS spectra it is possible to have information on the site structure by using the polarization of synchrotron light. In fact the effective coordination number depends on the photon polarization and incidence angle because θ_i is the angle between the electric vector of X-rays at the central atom site and the vector R_i from the central atom to the ith atom of the first shell. The comparison between the amplitudes of the surface EXAFS and that of the model compound $A(k)_m$ gives

$$\ln (A(k)_m/A(k)) = \ln (N^*_m R^2/N^* R^2_m) + 2k^2(\sigma^2 - \sigma^2_m) .$$

The term $2(R - R_m)/\lambda(k)$ can be omitted because $2|R - R_m| << \lambda(k)$. A linear plot of $\ln A(k)_m/A(k)$ vs k^2 yields the unknown coordination number N^* from the ordinate intercept at $k = 0$ and the σ^2 from the slope of the plot. In SEXAFS experiments the model can be the bulk.

The surface Debey-Waller factors determining the damping of surface EXAFS oscillations are expected to be different from that of the bulk. For example the calculated ratio of the surface-to-bulk mean-square displacements can be about 2 for the (100) surface of tungsten[69].

Several chemisorption sites have been studied with polarized synchrotron radiation. The adsorbate-substrate distances are determined using p-polarized X-rays and absorbate-adsorbate distances with s-polarized light. Also the number of substrate atoms bound to the adsorbed atom is found from the analysis of EXAFS amplitude of polarized spectra at several incidence angles.

5.1. - SEXAFS of chemisorption sites.

a) SEXAFS of Br_2 and Kr on graphite[13]. The SEXAFS of Br (K-edge) show that Br_2 molecule lies parallel to the surface plane. The Br-Br distance increases about 0.03 Å from the vapor. This result is confirmed by the angular dependence of a strong "shape resonance" in the near edge structures of the Br_2 molecule like that of N_2[5] Br-Br and Br-C EXAFS oscillations can be easily separated for their quite different behaviour of EXAFS amplitudes A(k). In this experiment the X-ray transmission has been measured.

b) SEXAFS of Oxygen chemisorbed on semiconductor and metal single crystals (O, K-edge). Using a grazing incidence monochromator in the soft-X-ray range[39] the SEXAFS of chemisorbed oxygen have been collected using partial yield, intermediate energy electron yield and total yield. This last detection method gives the best signal-to-noise ratio for SEXAFS[31, 32] and the spectra are free from interference with core direct photoemitted electrons over a large energy range. Fig. 12 shows SEXAFS spectrum of oxygen on Si(111) surface measured by Stöhr et al.[38] by secondary electron yield technique. A Si-O interatomic distance of 1.65 ± ± 0.03 Å has been extracted and an effective coordination number $N^* = 1.1$ has been found, to be compared with the values for the SiO_2 model compound $R_m = 1.61$ Å and $N^* = 2$. A larger Debey-Weller like factor has been found in the chemisorbed oxygen than in the bulk oxide.

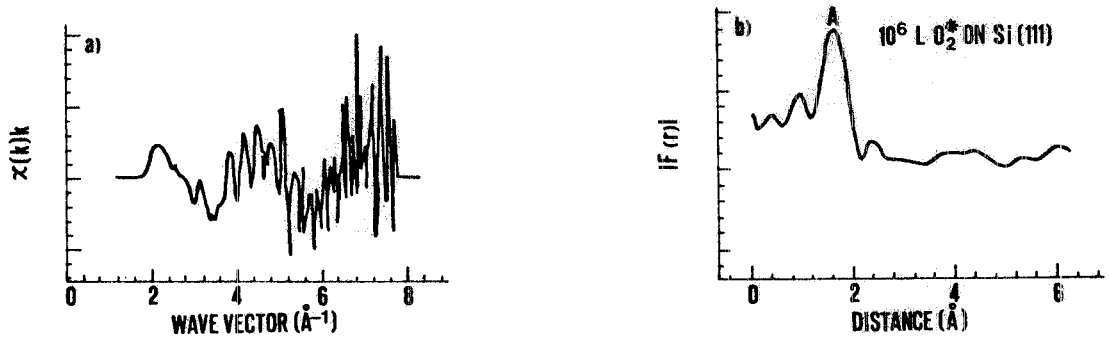

FIG. 12 - Surface EXAFS spectrum of oxygen chemisorbed on Si(111). The figure b) shows the module of the Fourier transform with mainly only one peak A corresponding to the first coordination shell. From reference (38).

A careful study of O on Al(111) has been performed by Stöhr et al.[31, 32, 70, 74]. The oxigen chemisorbs in the threefold hollow site with an interatomic Al-O distance $R = 1.76 \pm 0.03$ Å, which is much shorter than expected from LEED data. This distance remains unchanged from the half monolayer to the monolayer coverage. Also the O-O distance of the adsorbate monolayer has been measured[31, 32].

The chemisorption of oxygen on GaAs has been found to be dissociative[46] and the interatomic distance has been determined.

c) The SEXAFS of I_2 chemisorption on single crystal surfaces of Ag and Cu have been measured by Citrin et al.[71]. The I K-edge spectra have been recorded using a focused X-ray beam (collecting 10 mrad) and a Ge(111) crystal monochromator. From the analysis of A(k) they have been able to distinguish atomic or molecular chemisorption. The dependence of chemisorption sites on adsorbate coverage has also been studied.

5.2. - Surface EXAFS of clean crystals.

The surface EXAFS of a clean aluminum crystal has been measured by using the intermediate energy electron yield. By recording the secondary electron yield the bulk absorption spectrum is measured in the case of a clean surface. Therefore a direct comparison is possible between bulk and surface spectra taken on the same sample. Unfortunately it was possible to measure the surface EXAFS only in a short energy range at the L edge of Al. The results are shown in Fig. 13[47].

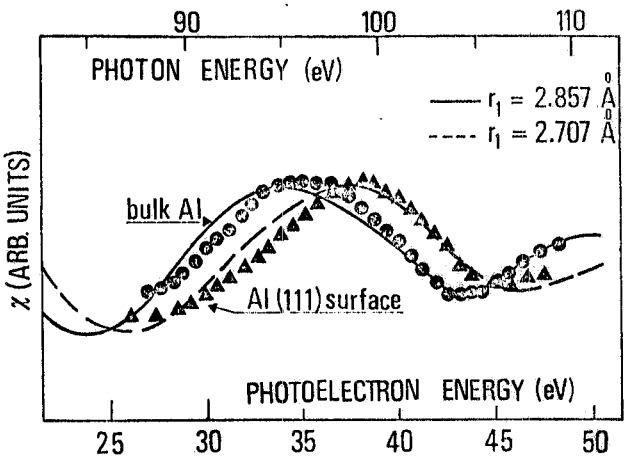

FIG. 13 - The first oscillation of bulk aluminum $L_{2,3}$ EXAFS and of Al(111) surface EXAFS. The solid curves are the calculated EXAFS oscillations for the bulk interatomic distance 2.857 Å and for the relaxed distance 2.707 Å; $(2.5 < k(Å^{-1}) < 3.5)$.

The data indicate a surface relaxation on the Al(111) surface of 0.15 Å. The surface sensitivity of this data is very high because it is determined by the effective escape depth of 45 eV electrons (see Fig. 5) which remains constant during the measurement. The electron are collected using the geometry shown in Fig. 4 with grazing incident p-polarized light. The surface sensitivity of these data should be higher than the LEED data where the energy of electrons is continuously changed. In the described experimental geometry (see Fig. 4) only the underlying atoms, as it is shown in Fig. 14, should contribute to the EXAFS oscillations.

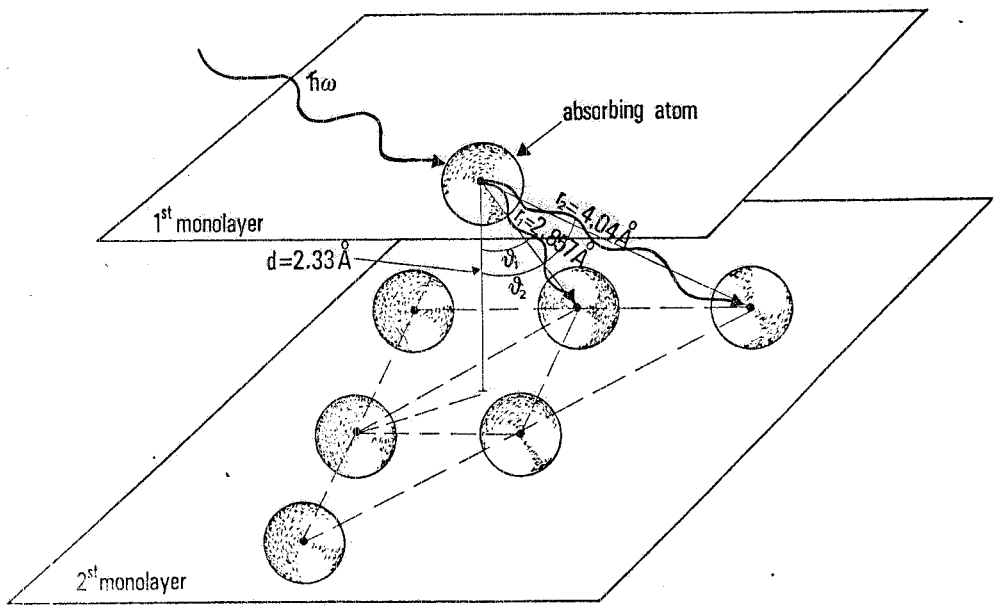

FIG. 14 - Surface structure of the Al(111) surface. The central atom on the first surface monolayer is sourounded by 6 atoms and it has 3 first neighbours at the same distance on the second monolayer. For p-polarized X-rays at grazing incidence only these last 3 atoms contribute to EXAFS.

The surface EXAFS of graphite has been extracted from angular integrated CIS spectrum of the 2s level at 19 eV binding energy below the Fermi level. After removing the smooth background from the raw data shown in ref. (59), a $\chi(k)$ curve has been obtained and plotted in Fig. 15. This experimental curve has been fitted with a single EXAFS sinusoidal oscillation giving a surface C-C distance, R = 1.41 Å which is the interatomic distance of carbon atoms on the graphite planes. The experimental geometry was that shown in Fig. 4 but no effects due to backscattering from the far underlying layers are observed.

The effects due to photoelectron diffraction for the limited solid angle collected by the CMA electron analyser have not been observed. Also the effects due to resonances of the asymmetry parameter $\beta(\hbar\omega)$ (see Section 3.4) can be disregarded. In fact β has been calculated[72] for the C 2s photoionization and large energy dependent deviation from 2 have been found only below 50 eV outside the energy range of the plotted EXAFS oscillations.

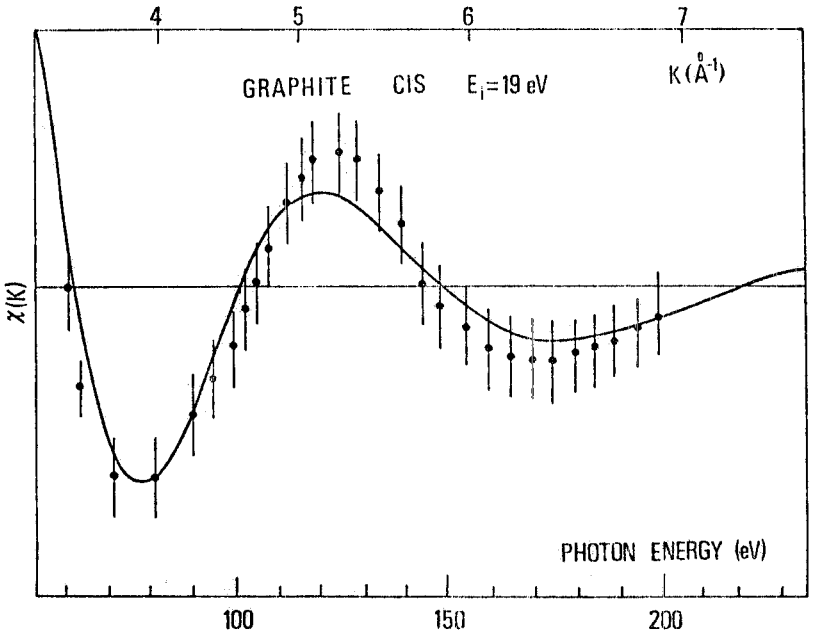

FIG. 15 - Surface EXAFS of graphite single crystal measured by recording the angular integrated constant initial state (CIS) spectrum of the 2s level at the initial state energy E_i = 19 eV.

Despite that there are some theoretical problems in the interpretation of the angular integrated CIS spectra it is important that simple EXAFS oscillations can be extracted from CIS spectra of the 2s level of C. In fact the carbon K spectra are very difficult to measure, they extend over a photon energy range ($h\nu \sim 280$ eV) which is generally not available due to carbon contamination on monochromator surfaces[73]. On the contrary C-2s angular integrated CIS spectra of chemisorbed molecules on metals, which are very important in surface science, can be measured in an available soft X-ray range at a synchrotron radiation facility.

6. - CONCLUSIONS.

SEXAFS and surface XANES are promising methods for surface structure determinations. These two spectroscopies give complementary information and they are both useful to clarify different aspects of chemisorption sites. Development of theories for interpretation of XANES is the next step in development of this spectroscopy. Development of techniques to measure SEXAFS spectra with both surface sensitivity and high signal-to-noise ratio is under way. Also the development of dedicated high current storage rings, wigglers and focused X-ray beamlines will allow in the next future to apply this new method to many surface physics and chemistry problems.

REFERENCES.

(1) - E. A. Stern, Contemp. Phys. 19, 289 (1978); P. Eisenberger and P. M. Kincaid, Science 200, 1441 (1978); E. E. Koch, C. Kunz and B. Sonntag, Phys. Rev. C29, 155 (1977).
(2) - C. J. Davisson and L. H. Germer, Phys. Rev. 30, 705 (1927); J. B. Pendry, Low Energy Electron Diffraction (Academic Press, 1974); P. Jona, Surface Sci. 68, 204 (1977).
(3) - M. Belli, A. Scafati, A. Bianconi, S. Mobilio, L. Palladino, A. Reale and E. Burattini, Solid State Comm. 35, 355 (1980).
(4) - P. J. Durham, J. B. Pendry and C. H. Hodges, Solid State Comm., to be published.
(5) - A. Bianconi, H. Petersen, F. C. Brown and R. Z. Bachrach, Phys. Rev. A17, 1907 (1978).
(6) - J. L. Dehmer and D. Dill, J. Chem. Phys. 65, 5327 (1967).
(7) - C. R. Natoli, F. W. Kutzler, D. K. Misemer and S. Doniach, Phys. Rev. A22, 1104 (1980).
(8) - A. Bianconi, S. Doniach and D. Lublin, Chem. Phys. Letters 59, 121 (1978).
(9) - B. K. Teo and P. A. Lee, J. Amm. Chem. Soc. 101, 2815 (1979).
(10) - P. Rabe, Japan. J. Appl. Phys. 17, Suppl. 17-2, 22 (1978).
(11) - J. J. Rehr, E. A. Stern, R. L. Martin and E. R. Davidson, Phys. Rev. B17, 560 (1978); Phys. Rev B, in press.
(12) - R. F. Pettifer, Proc. of the Intern. Conf. on X-ray Processes and Inner-shell Ionization, Stirling 1980 (to be published).
(13) - E. A. Stern, D. E. Sayers, J. G. Dash, J. Shechter and B. Bunker, Phys. Rev Letters 38, 767 (1977); S. M. Heald and E. A. Stern, Phys. Rev. B17, 4069 (1979).
(14) - R. Barchewitz, M. Cremonese-Visicato and G. Onori, J. Phys. C: Solid State Phys. 11, 4439 (1978).
(15) - D. Denley, P. Perfetti, R. S. Williams and D. A. Shirley, Phys. Rev. B21, 2267 (1980).
(16) - G. Martens and P. Rabe, Proc. of the Intern. Conf. on X-ray Processes and Inner-shell Ionization, Stirling 1980 (to be published.
(17) - R. Fox and S. J. Gurman, J. Phys. C: Solid State Phys. 13, L249 (1980).
(18) - J. Jaklevic, J. A. Kirby, M. P. Klein, A. S. Robertson, G. S. Brown and P. E. Eisenberger, Solid State Comm. 23, 679 (1977).
(19) - R. Z. Bachrach, R. S. Bauer, J. C. McMenamin and A. Bianconi, Physics of Semiconductors (Inst. of Physics, London, Conf. Ser. 43, 1979), p. 1073.
(20) - K. L. I. Kobayashi, private communication.
(21) - C. J. Powell, R. J. Stein, P. B. Needham Jr. and T. J. Driscoll, Phys. Rev. B16, 1370 (1977).
(22) - P. Pianetta, I. Lindau, C. M. Gardner and W. E. Spicer, Phys. Rev. B18, 2792 (1978).
(23) - R. S. Bauer, J. C. McMenamin, R. Z. Bachrach, A. Bianconi, L. Johansson and H. Petersen, Physics of Semiconductors (Inst. of Physics, London, Conf. Ser. 43, 1979), p. 797.
(24) - U. Bonse, DESY Report SR 78/29 (1978).
(25) - U. Landman and D. L. Adams, Proc. Nat. Acad. Sci. 73, 2550 (1976).
(26) - P. A. Lee, Phys. Rev B13, 5261 (1976); P. H. Citrin, P. Eisenberger and R. C. Hewitt, Phys. Rev. Letters 41, 309 (1978).
(27) - A. P. Lukirskii, O. A. Ershow, T. M. Zimkina and E. P. Savinov, Sov. Phys. - Solid State 8, 1422 (1966) A. P. Lukirskii and I. A. Brytov, Sol. Phys. Solid State 6, 33 (1964).
(28) - I. A. Britov and Yu. N. Romashenko, Sov. Phys. - Sol. State 20, 384 (1975).
(29) - W. Gudat and C. Kunz, Phys. Rev. Letters 29, 169 (1972).
(30) - G. Martens, P. Rabe, G. Tokiem and A. Werner, J. Phys. C: Solid State Phys. 11, 3125 (1978); DESY Report 79/15 (1979).
(31) - L. I. Johansson, J. Stöhr and S. Brennan, Applications of Surface Science, presented at this Conference.
(32) - J. Stöhr, L. I. Johansson, S. Brennan, M. Hecht and J. N. Miller, Phys. Rev. B (to be published).
(33) - W. Gudat and D. E. Eastman, Photoemission from Surfaces, ed. by. B. Feuerbacher, B. Fitton and R. F. Willis (Wiley, 1977), Chap. 11; D. E. Eastman and J. L. Freeouf, Phys. Rev. Letters 33, 1601 (1974).
(34) - D. L. Henke, J. Liesegang and S. D. Smith, Phys. Rev. B19, 3004 (1979).
(35) - J. Stöhr, D. Denley and P. Perfetti, Phys. Rev. B18, 4132 (1978).
(36) - J. Stöhr, J. Vac. Sci. Technol. 16, 37 (1979).
(37) - J. Stöhr, Japan. J. Appl. Phys. 17, 217 (1978).

(38) - J. Stöhr, L. Johansson, I. Lindau and P. Pianetta, Phys. Rev. B20, 664 (1979).
(39) - F. C. Brown, R. Z. Bachrach and N. Lien, Nuclear Instr. and Meth. 152, 73 (1978).
(40) - A. Bianconi, R. Z. Bachrach and S. A. Flodström, Solid State Comm. 24, 539 (1977).
(41) - A. Bianconi, R. Z. Bachrach and S. A. Flodström, Phys. Rev. B19, 3879 (1979).
(42) - A. Bianconi, R. Z. Bachrach, S. B. M. Hagstrom and S. A. Flodström, Phys. Rev. B19, 2837 (1979).
(43) - A. Bianconi, Surface Sci. 89, 41 (1979).
(44) - A. Bianconi and R. S. Bauer, Surface Sci. 99, 76 (1980).
(45) - R. Z. Bachrach, D. J. Chadi and A. Bianconi, Solid State Comm. 28, 931 (1978).
(46) - J. Stöhr, R. S. Bauer, J. C. McMenamin, L. I. Johansson and S. Brennan, J. Vac. Sci. Technol. 16, 1195 (1979).
(47) - A. Bianconi and R. Z. Bachrach, Phys. Rev. Letters 42, 104 (1979).
(48) - M. L. Knotek, V. O. Jones and V. Rehn, Phys. Rev. Letters 43, 300 (1979).
(49) - R. Franchy and D. Menzel, Phys. Rev. Letters 43, 865 (1979).
(50) - J. Stöhr et al., ECOSS 3 Conference, Cannes 1980 (unpublished).
(51) - M. L. Knotek, V. O. Jones and V. Rehn, to be published.
(52) - A. Bianconi, D. Jackson and K. Monahan, Phys. Rev. B17, 2021 (1978).
(53) - G. P. Lapeyre, A. D. Baer, J. Hermanson, J. Anderson, J. A. Knapp and P. L. Gobby, Solid State Comm. 15, 1601 (1974).
(54) - E. Dietz and D. E. Eastman, Phys. Rev. Letters 41, 1674 (1978).
(55) - C. H. Li and S. Y. Tong, Phys. Rev. Letters 43, 526 (1979); 42, 901 (1979).
(56) - S. D. Kevan, D. H. Rosenblatt, D. R. Denley, B. C. Lu and D. A. Shirley, Phys. Rev. B20, 4133 (1979).
(57) - I. Lindau, P. Pianetta and W. E. Spicer, Phys. Letters 57A, 225 (1976).
(58) - R. Z. Bachrach and A. Bianconi, Proc. V Intern. Conf. on Vacuum Ultraviolet Radiation Physics, Montpellier (1977), Vol. II, p. 213.
(59) - A. Bianconi, S. B. M. Hagström and R. Z Bachrach, Phys. Rev. B16, 5543 (1977).
(60) - G. Margaritondo and N. G. Stoffel, Phys. Rev Letters 42, 1567 (1979).
(61) - A. F. Starace, R. H. Rast and S. T. Manson, Phys. Rev. Letters 38, 1522 (1977).
(62) - M. L. den Boer, T. L. Einstein, W. T. Elam, R. L. Park, L. D. Roelofs and G. E. Laramore, Phys. Rev. Letters 44, 496 (1980).
(63) - W. T. Elam, P. I. Cohen, L. Roelofs and R. L. Park, Appl. of Surface Sci. 2, 636 (1979); P. I. Cohen, T. L. Einstein, W. T. Elam, Y. Fukuda and R. L. Park, Appl. of Surface Sci. 1, 538 (1978).
(64) - G. E. Laramore, T. L. Einstein, L. D. Roelofs and R. L. Park, Phys. Rev. B21, 2108 (1980).
(65) - G. E. Laramore, T. L. Einstein and R. L. Park, Proc. Intern. Conf. on X-ray Processes and Inner-shell Ionization, Stirling 1980 (to be published).
(66) - J. P. Connerade, Contemporary Physics 19, 415 (1978).
(67) - A. Bianconi, S. Modesti, M. Campagna and S. Stizza, Solid State Comm., in press; P. S. Wei and F. W. Lytle, Phys. Rev. B19, 679 (1979).
(68) - K. Hübner, Phys. Status Solidi A40, 133 and 487 (1977); K. Hübner and A. Lehmann, Phys. Status Solidi A46, 451 (1978); R. N. Nucho and A. Madhukar, Phys. Rev. B21, 1576 (1980).
(69) - R. F. Wallis and D. J. Cheng, Solid State Comm. 34, 847 (1980).
(70) - L. I. Johansson and J. Stöhr, Phys. Rev Letters 43, 1882 (1979); S. Brennan, R. Jaeger and J. Stöhr, VI Intern. Conf. on Vacuum Ultraviolet Radiation Physics, Charlottesville 1980 (unpublished).
(71) - P. H. Citrin, P. Eisenberger and R. C. Hewitt, Surface Sci. 89, 28 (1979); Phys. Rev. Letters 45, 1948 (1980).
(72) - E. S. Chang and K. T. Taylor, Daresbury Laboratory Report DL/SRF/P 132.
(73) - F. C. Brown, R. Z. Bachrach and A. Bianconi, Chem. Phys. Letters 54, 425 (1978).
(74) - D. Norman, S. Brennan, R. Jaeger and J. Stöhr, Surface Sci. Letters, to be published.